# Transient Eddy Forcing of the Time-Mean Flow as Identified by Geopotential Tendencies

NGAR-CHEUNG LAU

*Geophysical Fluid Dynamics Program, Princeton University, Princeton, NJ 08540*

EERO O. HOLOPAINEN

*Department of Meteorology, University of Helsinki, 00100 Helsinki 10, Finland*

(Manuscript received 13 June 1983, in final form 11 October 1983)

ABSTRACT

The forcing of the time-mean flow by transient eddies is examined within the framework of a quasi-geostrophic equation relating the geopotential tendency to the convergence of transient eddy transports of heat and vorticity. The forcing functions of this equation are computed using observed circulation statistics for the wintertime Northern Hemisphere, and solutions are sought for the three-dimensional structure of geopotential and temperature tendencies associated with eddies of different time scales.

In general, the geopotential tendencies associated with vorticity fluxes are of the same sign within a given atmospheric column; whereas the polarity of the geopotential tendencies associated with heat fluxes in the lower troposphere is opposite to that in the upper troposphere. The geostrophic wind tendencies associated with synoptic-scale eddies with periods between 2.5 and 6 days are strongest in the vicinity of the oceanic storm tracks. The enhanced poleward heat transports by active disturbances in these regions lead to eastward accelerations of the geostrophic flow in the lower troposphere, westward accelerations in the upper troposphere, and hence a reduction in the vertical shear of the eastward flow along the storm tracks. The vorticity transports by eddies with synoptic time scales are associated with eastward accelerations throughout the troposphere over the storm tracks. The geostrophic wind tendencies associated with the vorticity fluxes tend to dominate in the upper troposphere, so that the combined effect of the eddy transports of heat and vorticity by synoptic-scale eddies is to accelerate the eastward current at all vertical levels in middle latitudes. The geopotential tendencies associated with eddies with periods between 10 days and a season are generally stronger than those associated with synoptic-scale disturbances. In the upper troposphere, the transports of both heat and vorticity by the low-frequency eddies are accompanied by tendencies which act to destroy the departure from zonal symmetry of the time-averaged geopotential height field. The forcing of the geopotential height field due to vorticity transports by low-frequency eddies is stronger than the corresponding forcing due to heat transports.

The temperature tendencies associated with eddy heat transports are much stronger than those associated with eddy vorticity transports. The thermal forcing due to synoptic-scale disturbances is characterized by dipole-like structures over the western oceans, with positive temperature tendencies (warming) north of the cyclone tracks and negative tendencies (cooling) further south. In the lower troposphere, the tendencies associated with low-frequency eddies act to destroy the zonally asymmetric component of the stationary temperature field. The typical magnitude of temperature tendencies as computed using the present method, which implicitly takes into account the combined effects of eddy flux convergences and the associated secondary circulations, is about 60–70% of the corresponding values obtained by considering the convergence of eddy heat fluxes alone.

The effects of transient disturbances as depicted by tendencies associated with eddy fluxes are contrasted with earlier results based on eddy transports of quasi-geostrophic potential vorticity. The distinction between these two approaches is discussed.

## 1. Introduction

The effect of transient eddies (hereafter abbreviated as TE) on the time-mean state is a fundamental problem in theoretical and observational studies of the general circulation of the atmosphere. TE influence the atmospheric state by redistributing heat and vorticity in a systematic fashion. The contributions of TE to time-averaged balances may formally be expressed in terms of the convergences of eddy fluxes. However, hydrostatic and geostrophic constraints require that these TE fluxes operate in conjunction with secondary circulations (e.g., see Holton, 1979, Chap. 10), which also affect the time-mean atmospheric state. A comprehensive treatment of the *net* effect of TE on the mean flow must therefore take into consideration not only the convergences of TE fluxes, but also the influences of the eddy-induced circulations.

The above problem may in principle be approached by treating the convergences of TE fluxes as virtual sources and sinks of heat and vorticity, and solving for the stationary response to these forcing functions. This methodology has been adopted by Youngblut and Sasamori (1980) using a quasi-geostrophic model,

and by Opsteegh and Vernekar (1982) using a primitive equation model. Both studies indicate that the TE act to reduce the amplitude of the stationary waves forced by orography. However, quantitative estimates of these dissipative effects appear to be rather sensitive to the particular model approximations used.

Instead of seeking finite-amplitude solutions to the time-mean equations, considerable insight into the nature of TE effects could also be gained by examining the initial atmospheric response at the instant when the eddy forcing is imposed. If the primitive equations were used to study this problem, one would obtain initial tendencies which generate small-scale noise of no real meteorological interest. A more useful framework for the present purpose would be the quasi-geostrophic system, which ensures that the initial tendencies are in hydrostatic and geostrophic balance.

The initial tendencies associated with both transient and stationary eddies in a zonally averaged atmosphere have been examined by Wiin-Nielsen and Vernekar (1967) and Pfeffer (1981). The eddy-induced meridional circulation was computed by solving a diagnostic equation relating the streamfunction for that circulation to the eddy forcing terms. The effects of this secondary circulation were then combined with the convergences of eddy fluxes to yield the net influence of transient and stationary eddies on the zonal wind and temperature fields. It was found that maximum eastward acceleration of the zonal flow by the eddies occurs poleward of the zonally averaged jet core, and that the eddies generally tend to diminish the meridional temperature gradient in the troposphere.

In the present study, the effects of TE on the time-mean flow are diagnosed using the quasi-geostrophic potential vorticity equation. The eddy forcing terms in this equation are evaluated using observed circulation statistics for the winter season in the Northern Hemisphere. This quasi-geostrophic system, together with appropriate boundary conditions, are then solved for the three-dimensional distributions of geopotential height, geostrophic wind and temperature tendencies associated with the eddies. The initial tendencies thus obtained satisfy the hydrostatic and geostrophic constraints, so that the contributions of both the eddy-induced circulations and the eddy flux convergences have already been taken into account. The present approach is hence equivalent to that used by Wiin-Nielsen and Vernekar (1967) and Pfeffer (1981), who considered the eddy-induced circulations and eddy flux convergences separately. Furthermore, the results to be presented here extend beyond the scope of earlier studies by 1) considering the effects of eddy fluxes both in the interior and at the boundaries, 2) highlighting the geographical distribution of the TE forcing, 3) differentiating the roles of eddy heat fluxes and eddy vorticity fluxes, and 4) assessing the contributions to TE forcing by fluctuations of various time scales.

The quasi-geostrophic system may also be diagnosed from a perspective which is quite distinct from that outlined above. Holopainen *et al.* (1982, hereafter referred to as A) have depicted the regional effects of TE with the aid of a nondivergent vector field $\mathbf{F}_\psi$, which is related to the potential function for the eddy flux of quasi-geostrophic potential vorticity (see Section 8). The zonal mean of the east-west component of $\mathbf{F}_\psi$ may be equated to the divergence of the Eliassen–Palm flux, and is hence one measure of the net TE forcing of the zonally averaged flow (Edmon *et al.*, 1980). It was reported in A that $\mathbf{F}_\psi$ is almost everywhere directed against the local time-averaged flow in the middle and upper troposphere.

The quasi-geostrophic framework is introduced in Section 2. Analytic solutions to a set of simplified equations with idealized eddy forcings are presented in Section 3, so as to gain some qualitative insight into the nature of TE forcing. Those readers who are primarily interested in the observational results may reserve much of the details in Section 3 for a later reading, and proceed immediately from Section 2 to Section 4 without much loss of continuity. The observational data base and the numerical method used in solving the quasi-geostrophic equation are described in Section 4. In Section 5 are shown hemispheric distributions of geopotential and geostrophic wind tendencies accompanying transports of heat and vorticity by eddies of different time scales. The corresponding results for temperature tendencies are discussed in Section 6. The zonally averaged distributions of the zonal wind and temperature tendencies are presented in Section 7 and compared with results from other studies. In Section 8 the results on initial tendencies as reported here are contrasted with those on TE fluxes of potential vorticity as reported in A.

## 2. Basic equations

For the present purpose, the quasi-geostrophic potential vorticity equation may be written as [refer to Holton (1979, Chap. 6) for a detailed derivation]

$$\left\{\frac{1}{f}\nabla^2 + f\frac{\partial}{\partial p}\left(\frac{1}{\sigma}\frac{\partial}{\partial p}\right)\right\}\frac{\partial \Phi}{\partial t} = D + R_1, \tag{1}$$

where $\Phi$ is the geopotential, $t$ the time variable, $f$ the Coriolis parameter, $\sigma = -(\alpha/\theta)(\partial\theta/\partial p)$ the static stability parameter, assumed to be a function of pressure $p$ only, $\theta$ the potential temperature, and $\alpha$ the specific volume. All terms associated with TE fluxes are contained in $D$, which may be expressed as (see A for details)

$$D = D^{\mathrm{HEAT}} + D^{\mathrm{VORT}}, \tag{2}$$

where

$$D^{\mathrm{HEAT}} = f\frac{\partial}{\partial p}\left(\frac{\nabla\cdot\overline{\mathbf{V}'\theta'}}{\tilde{S}}\right) \tag{3}$$

$$D^{\mathrm{VORT}} = -\nabla\cdot\overline{\mathbf{V}'\zeta'}. \tag{4}$$

Here the overbar represents a time average, and the prime represents deviations from the corresponding time-averaged quantity; $\tilde{S}$ is the hemispheric mean of the quantity $-\partial\bar{\theta}/\partial p$, V is the horizontal velocity, and $\zeta$ the relative vorticity. The term $R_1$ in Eq. (1) represents all remaining components in the quasi-geostrophic potential vorticity balance, such as horizontal advection by the time mean flow, diabatic effects and friction.

The conditions to be satisfied by $\partial\Phi/\partial t$ at the lower and upper boundaries are specified by the thermodynamic energy equation

$$-\frac{p}{R}\left(\frac{p_0}{p}\right)^{R/C_p}\frac{\partial}{\partial p}\left(\frac{\partial\Phi}{\partial t}\right) = -\nabla\cdot\overline{\mathbf{V}'\theta'} + R_2. \quad (5)$$

Here $p_0 = 1000$ mb, $R$ is the gas constant, $C_p$ the heat capacity at constant pressure, and $R_2$ represents all remaining terms in the heat balance, such as horizontal and vertical advection by the time mean flow and diabatic effects.

Since the present investigation is solely concerned with the initial response of a quasi-geostrophic atmosphere to eddy forcing represented by $D$ in Eq. (1) and $-\nabla\cdot\overline{\mathbf{V}'\theta'}$ in Eq. (5), we may set

$$R_1 = R_2 = 0.$$

Hence Eq. (1) may be simplified as

$$\left\{\frac{1}{f}\nabla^2 + f\frac{\partial}{\partial p}\left(\frac{1}{\sigma}\frac{\partial}{\partial p}\right)\right\}\left(\frac{\partial\Phi}{\partial t}\right)_{\mathrm{TE}} = D, \quad (6)$$

where $(\partial\Phi/\partial t)_{\mathrm{TE}}$ denotes the initial geopotential tendency due to the combined effects of TE heat fluxes and vorticity fluxes. The corresponding tendencies of geostrophic wind $(\partial\mathbf{V}/\partial t)_{\mathrm{TE}}$ and temperature $(\partial T/\partial t)_{\mathrm{TE}}$ are determined from $(\partial\Phi/\partial t)_{\mathrm{TE}}$ by setting

$$\left(\frac{\partial\mathbf{V}}{\partial t}\right)_{\mathrm{TE}} = \frac{1}{f}\mathbf{k}\times\nabla\left(\frac{\partial\Phi}{\partial t}\right)_{\mathrm{TE}},$$

$$\left(\frac{\partial T}{\partial t}\right)_{\mathrm{TE}} = -\frac{p}{R}\frac{\partial}{\partial p}\left(\frac{\partial\Phi}{\partial t}\right)_{\mathrm{TE}}.$$

Here, $\mathbf{k}$ is the unit vector in the vertical direction. Eq. (6) may also be solved for the tendency associated individually with heat fluxes $(\partial\Phi/\partial t)_{\mathrm{TE}}^{\mathrm{HEAT}}$ and with vorticity fluxes $(\partial\Phi/\partial t)_{\mathrm{TE}}^{\mathrm{VORT}}$. This may be accomplished by inserting the corresponding forcing $D^{\mathrm{HEAT}}$ and $D^{\mathrm{VORT}}$ separately in Eq. (6), instead of their sum $D$. From Eq. (5), the appropriate conditions for $(\partial\Phi/\partial t)_{\mathrm{TE}}^{\mathrm{HEAT}}$ and $(\partial\Phi/\partial t)_{\mathrm{TE}}^{\mathrm{VORT}}$ at the upper and lower boundaries are

$$-\frac{p}{R}\left(\frac{p_0}{p}\right)^{R/C_p}\frac{\partial}{\partial p}\left(\frac{\partial\Phi}{\partial t}\right)_{\mathrm{TE}}^{\mathrm{HEAT}} = -\nabla\cdot\overline{\mathbf{V}'\theta'}, \quad (7)$$

$$\frac{\partial}{\partial p}\left(\frac{\partial\Phi}{\partial t}\right)_{\mathrm{TE}}^{\mathrm{VORT}} = 0. \quad (8)$$

In writing the above equations, it has been assumed that the eddy-induced vertical velocity vanishes at the boundaries. It is worth noting here that identical solutions for $(\partial\Phi/\partial t)_{\mathrm{TE}}$ may be obtained by a method analogous to the zonal mean calculations by Pfeffer (1981). The latter approach entails the solution of a three-dimensional omega-equation for the eddy-induced vertical velocity $\omega_{\mathrm{TE}}$, again subject to the condition that $\omega_{\mathrm{TE}} = 0$ at the boundaries. The divergence associated with $\omega_{\mathrm{TE}}$ could subsequently be combined with $D^{\mathrm{VORT}}$ to yield the net effect of TE in altering the local vorticity. The vorticity tendency thus obtained may then be expressed in terms of $(\partial\Phi/\partial t)_{\mathrm{TE}}$.

## 3. Some analytic solutions for a simplified system

Prior to the presentation of solutions of Eqs. (6)–(8) for observed TE forcing, it is helpful to gain some qualitative insight by considering the analytic solutions corresponding to idealized eddy forcings. We shall use a simplified version of Eq. (6)

$$\left(\frac{1}{f_0}\nabla^2 + \frac{f_0}{\sigma}\frac{\partial^2}{\partial p^2}\right)\left(\frac{\partial\Phi}{\partial t}\right)_{\mathrm{TE}} = D, \quad (6')$$

where the static stability parameter $\sigma$ and the Coriolis parameter $f_0$ are to be treated as constants.

### a. Forcing by TE heat fluxes

We first assume that the convergence of TE transports increases linearly with pressure, i.e.,

$$\frac{-\nabla\cdot\overline{\mathbf{V}'\theta'}}{\tilde{S}} = Q(x, y)\left(\frac{p - p_T}{p_0 - p_T}\right),$$

so that

$$D_{\mathrm{TE}}^{\mathrm{HEAT}} = -f_0\frac{Q(x, y)}{p_0 - p_T}$$

is invariant with pressure. Here $p_0$ and $p_T$ denote respectively the pressure at the lower and upper boundaries, where the following conditions are to be satisfied:

$$\frac{\partial}{\partial p}\left(\frac{\partial\Phi}{\partial t}\right)_{\mathrm{TE}}^{\mathrm{HEAT}} = \begin{cases}0, & \text{at } p = p_T\\ -\sigma Q(x, y), & \text{at } p = p_0.\end{cases}$$

For solutions in $(x, y, p)$ coordinates of the form

$$\left(\frac{\partial\Phi}{\partial t}\right)_{\mathrm{TE}}^{\mathrm{HEAT}} = \mathrm{Re}[A(p)e^{i(kx+ly)}],$$

and letting

$$Q(x, y) = \mathrm{Re}[Q_0 e^{i(kx+ly)}],$$

Eq. (6′) may be written as

$$\frac{d^2A}{dp^2} - \mu^2 A = -\frac{\sigma Q_0}{\Delta p},$$

with boundary conditions

$$\frac{dA}{dp} = \begin{cases} 0, & \text{at } p = p_T \\ \sigma Q_0, & \text{at } p = p_0. \end{cases}$$

Here $\mu^2 = \sigma f_0^{-2}(k^2 + l^2) > 0$ and $\Delta p = p_0 - p_T$. The solution to the above system is given by

$$\left(\frac{\partial \Phi}{\partial t}\right)_{\text{TE}}^{\text{HEAT}} = \text{Re}\left\{\frac{\sigma Q_0}{\Delta p}\left[\underbrace{\frac{1}{\mu^2}}_{\text{I}} - \underbrace{\frac{\Delta p}{\mu}\frac{e^{\mu(p_T-p)} + e^{-\mu(p_T-p)}}{e^{\mu\Delta p} - e^{-\mu\Delta p}}}_{\text{II}}\right]e^{i(kx+ly)}\right\}.$$

Using the following parameters for the atmosphere at 45°N: $l = 0$, $\sigma = 10^{-5}$ m$^4$ s$^2$ kg$^{-1}$, $p_0 = 1000$ mb and $p_T = 100$ mb, the vertical variations of $(\partial\Phi/\partial t)_{\text{TE}}^{\text{HEAT}}$ over a location of maximum TE heat flux convergence are presented in Fig. 1. The two profiles shown here correspond to zonal wavenumbers 1 and 6, and are expressed in units of $\sigma Q_0/\Delta p$. It is found that terms I and II tend to cancel each other to a large extent. These strong cancellations may be demonstrated by the fact that, for zonal wavenumber 1, the maximum absolute value of $(\partial\Phi/\partial t)_{\text{TE}}^{\text{HEAT}}[2.6 \times 10^9\ (\sigma Q_0/\Delta p)$ mks units] is merely a small fraction of the constant value of term I [$2.2 \times 10^{10} \times (\sigma Q_0/\Delta p)$ mks units]. The solution shown in Fig. 1 implies that the convergence of eddy heat flux is accompanied by cyclonic tendencies in the lower troposphere, anticyclonic tendencies in the upper troposphere, and positive temperature tendencies (warming) throughout the troposphere. Additional calculations (not shown) indicate that the above conclusions hold for a wide range of the parameters $\sigma$ and $k$.

The configuration of geopotential and geostrophic wind tendencies associated with TE heat fluxes is depicted schematically in Fig. 2a. It is evident from this diagram that the irrotational component of the TE heat fluxes[1] tends to accelerate the geostrophic wind component perpendicular to the direction of the heat transport. The wind acceleration is directed to the right of the eddy heat flux in the lower troposphere, and to the left in the upper troposphere. If the line AB in Fig. 2a is visualized as a zonally oriented storm track over the midlatitude oceans, where the poleward heat transports associated with the enhanced synoptic-scale wave activities are observed to attain a maximum (Blackmon *et al.*, 1977), we would expect eastward acceleration of the geostrophic wind in the lower troposphere, westward acceleration in the upper troposphere, and warming (cooling) tendencies at locations poleward (equatorward) of the storm track. These qualitative considerations will aid our interpretation of the patterns to be presented in Sections 5 and 6 for tendencies associated with observed eddy forcing.

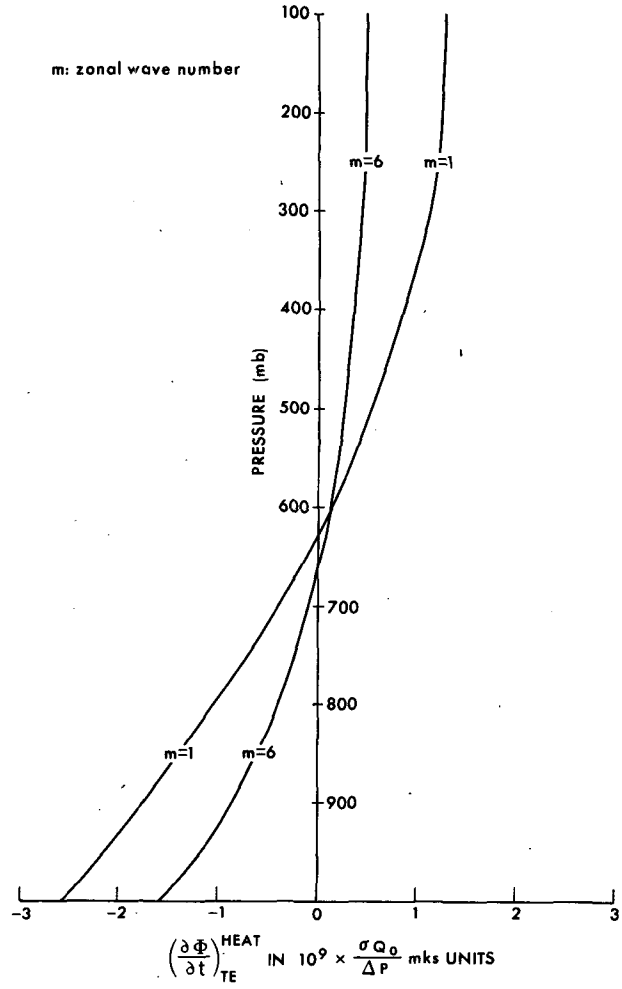


FIG. 1. Vertical profile of the geopotential tendency associated with an idealized forcing of TE heat fluxes described in the text, for an atmospheric column located at the site of maximum TE heat flux convergence.

### b. *Forcing by TE vorticity fluxes*

Assuming that the convergence of TE vorticity fluxes is independent of pressure, i.e.,

$$D^{\text{VORT}} = -\nabla \cdot \overline{\mathbf{V}'\zeta'} = \text{Re}[Be^{i(kx+ly)}],$$

where $B$ is a constant. Then, proceeding as before, the solution

$$\left(\frac{\partial \Phi}{\partial t}\right)_{\text{TE}}^{\text{VORT}} = \text{Re}[A(p)e^{i(kx+ly)}]$$

[1] The expansion of horizontal vector flux fields in terms of nondivergent and irrotational parts is discussed in further detail by Lau and Wallace (1979).

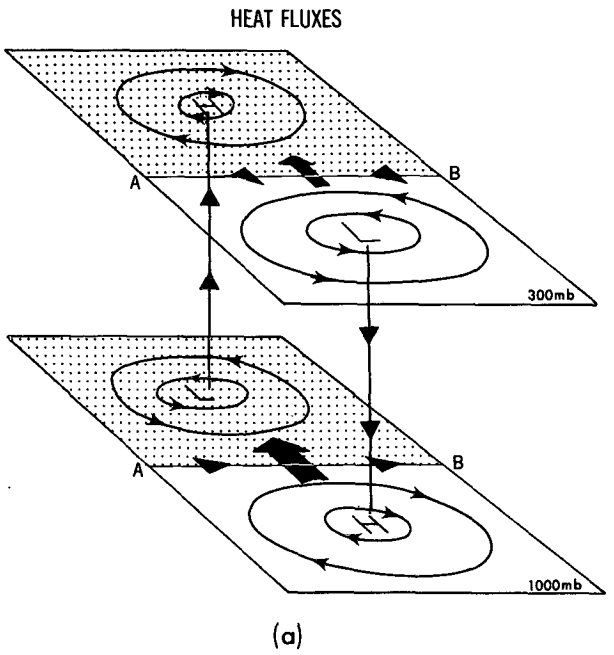


FIG. 2a. Schematic representation of the geopotential tendencies (contours) at 1000 mb (lower plane) and 300 mb (upper plane) associated with irrotational TE heat fluxes (arrows with bold shafts). The dotted and undotted halves of each plane indicate convergence and divergence of TE heat fluxes, respectively. Arrow heads on the horizontal planes indicate the direction of geostrophic wind tendencies. Arrow heads pointing in the vertical direction indicate the induced vertical motion in the middle troposphere.

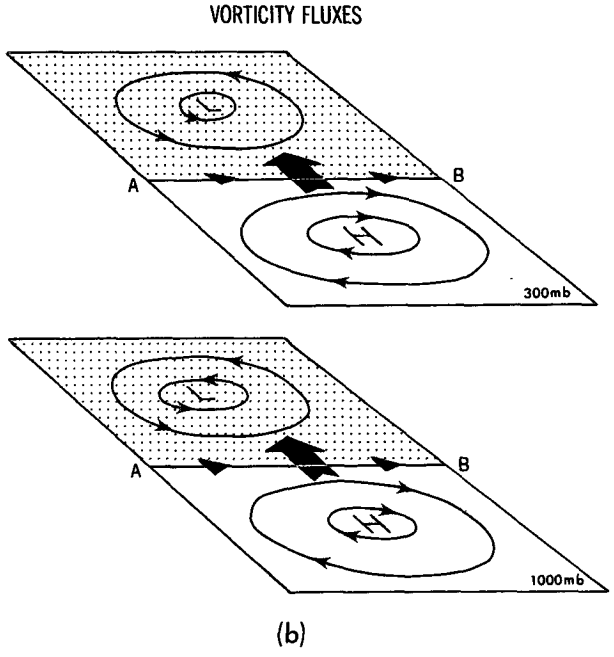


FIG. 2b. As in Fig. 2a, but for geopotential and wind tendencies associated with irrotational TE vorticity fluxes.

should satisfy

$$\frac{d^2A}{dp^2} - \mu^2 A = B,$$

with boundary conditions $dA/dp = 0$ at $p = p_0$ and $p = p_T$. It is readily seen that $A = -\mu^{-2}B$ and

$$\left(\frac{\partial \Phi}{\partial t}\right)_{\text{TE}}^{\text{VORT}} = \text{Re}\left[-\frac{B}{\mu^2} e^{i(kx+ly)}\right].$$

The geopotential tendency associated with $D^{\text{VORT}}$ is hence invariant with pressure and has a polarity opposite to that of the local vorticity flux convergence. A schematic representation of $(\partial\Phi/\partial t)_{\text{TE}}^{\text{VORT}}$ is given in Fig. 2b, which indicates that the irrotational component of the TE vorticity fluxes tends to accelerate the flow perpendicular to the direction of eddy transport. The acceleration is directed to the right of the vorticity flux at all levels. If the line AB is again viewed as the axis of a storm track, which corresponds closely to the site of maximum poleward irrotational TE vorticity transport (Lau and Wallace, 1979, Fig. 10b), the flow along the storm track would experience an eastward acceleration; whereas the thermal field would experience little change. These relationships will also be useful in the discussion pertaining to patterns for $(\partial\Phi/\partial t)_{\text{TE}}^{\text{VORT}}$ as computed for observed forcing.

## 4. The data set and procedure for numerical solution

The observational data set for this study consists of climatological statistics for TE heat and vorticity fluxes. These eddy statistics are computed using twice-daily gridded analyses produced operationally by the U.S. National Meteorological Center (NMC) during an eight-winter period (1966–67 to 1968–69, 1970–71 to 1974–75). The winter season is taken to be the 120-day period starting from 15 November. At the 1000 mb level, the wind and temperature data are derived from the geopotential height analyses using the geostrophic and hydrostatic relationships. The eddy statistics at all other pressure levels are compiled using the actual wind and temperature analyses. In order to distinguish transient phenomena of various time scales, the covariance statistics have been compiled on the basis of time series subjected to the following time-filters:

- A band-pass filter retaining fluctuations with periods between 2.5 and 6 days.
- A low-pass filter retaining fluctuations with periods between 10 days and a season.

The filtering procedure follows that described in Blackmon (1976). The NMC circulation statistics have been documented in detail by Lau *et al.* (1981).

The solutions to the Eqs. (6)–(8) were obtained by the following procedure:

1) The eddy forcing of interest ($D^{HEAT}$, $D^{VORT}$ or $D$), the heat flux convergence at the upper and lower boundaries, and the associated tendency

$$\left(\frac{\partial\Phi}{\partial t}\right)_{TE}^{HEAT}, \left(\frac{\partial\Phi}{\partial t}\right)_{TE}^{VORT} \quad \text{or} \quad \left(\frac{\partial\Phi}{\partial t}\right)_{TE}$$

were expressed as a sum of zonal harmonic components, with truncation at zonal wavenumber 10. This particular truncation has been selected so as to provide an adequate representation of all essential features appearing in the spatial patterns of the eddy forcing terms.

2) Eqs. (6)–(8) were rewritten in terms of the coefficients of individual harmonics. This yields altogether 21 sets of equations (one for the zonal mean, and two for each of the first ten wavenumbers). Each set consists of a separable elliptic equation with latitude and pressure as independent variables, as well as the expressions for the appropriate conditions to be satisfied at the upper and lower boundaries.

3) The harmonic coefficients for the eddy forcing terms were obtained by Fourier analysis of the NMC circulation statistics. The fourth-order finite difference approximation to the equations for each harmonic component was then solved using the computer subroutine SEPELI described in the NCAR Software Support Library (1976).

4) The geopotential tendency was finally assembled by summation of the solutions for individual harmonic components. The corresponding wind and temperature tendencies were then computed using the geostrophic and hydrostatic relationships.

In Eq. (6), the horizontal Laplacian has been expressed in spherical coordinates, $f$ was allowed to vary with latitude, and the vertical profile of $\sigma$ (function of pressure only) was determined from the NMC data. The equations were solved for the domain extending vertically from $p_0 = 1000$ mb to $p_T = 100$ mb, and meridionally from 20°N to 90°N. The boundaries of this particular domain are essentially determined by the spatial extent of the NMC analyses. The vertical and horizontal resolutions used were 50 mb and 2.5° latitude, respectively. The eddy forcing terms were first computed at standard pressure levels, and were then interpolated to the equally spaced levels using cubic splines. The boundary conditions at 20°N and 90°N were assumed to be

$$\left(\frac{\partial\Phi}{\partial t}\right)_{TE} = 0 \quad \text{and} \quad \frac{\partial}{\partial y}\left(\frac{\partial\Phi}{\partial t}\right)_{TE} = 0,$$

respectively. In view of the somewhat artificial condition imposed at 20°N, due caution should be exercised when interpreting the solution in the immediate vicinity of this latitude circle.

It is worth noting that, in solving for $(\partial\Phi/\partial t)_{TE}^{HEAT}$, results identical to those determined from Eqs. (6)–(7) may alternatively be obtained by ignoring the convergence of TE heat fluxes at the boundaries, i.e., by setting

$$\frac{\partial}{\partial p}\left(\frac{\partial\Phi}{\partial t}\right)_{TE}^{HEAT} = 0$$

in Eq. (7), *provided that* the corresponding eddy forcing $D^{HEAT}$ in Eq. (6) is also computed with the assumption $\nabla\cdot\overline{\mathbf{V}'\theta'} = 0$ at the same boundaries. That this alternative approach is consistent with Eqs. (6)–(7) may be seen from the pertinent finite-difference equations, and has also been verified by direct computation. This treatment of heat transports near horizontal boundaries is essentially similar to that used in the theoretical study by Bretherton (1966). The above considerations imply that the eddy heat fluxes at the boundaries need not be specified to a high precision. Hence the appreciable uncertainties to which the observed eddy statistics at 1000 mb may be subjected should not affect the accuracy of the solutions for $(\partial\Phi/\partial t)_{TE}^{HEAT}$.

## 5. Regional characteristics of geopotential and wind tendencies

### *a. Band pass fluctuations*

In Fig. 3 are shown the distributions of $(\partial\Phi/\partial t)_{TE}^{HEAT}$ and $(\partial\Phi/\partial t)_{TE}^{VORT}$ at 300 and 1000 mb, as computed using eddy statistics for band pass filtered data. The most notable features in these patterns are the dipole-like structures located over the western oceans. The centers of extremum for these dipoles tend to straddle the axis of the climatological storm tracks. These storm tracks (depicted by arrows with thick, dashed shafts in Fig. 3d) stretch eastward across the two ocean basins along the 45°N latitude during the winter season, and correspond to preferred sites for the development and passage of migratory cyclones (Blackmon *et al.*, 1977). It is seen that the heat transports by these synoptic-scale eddies are associated with westward acceleration of the local geostrophic flow in the upper troposphere, and eastward acceleration near the sea level (Figs. 3a and 3b). The TE heat fluxes hence act to diminish the vertical wind shear over the storm tracks. These results are consistent with the schematic representation shown in Fig. 2a.

The geopotential tendencies associated with TE vorticity fluxes (Figs. 3c and 3d) exhibit a distinct equivalent barotropic character. The strongest eastward accelerations take place at approximately 45°N, 160°E and 45°N, 70°W, where the synoptic-scale disturbances typically start to intensify. Noting that the irrotational component of the TE vorticity flux is directed poleward at these locations (Lau and Wallace, 1979, Fig. 10b), the observed patterns there agree quite well with the relationships portrayed in Fig. 2b.

Along the western portion of the oceanic storm tracks, the geostrophic wind accelerations associated

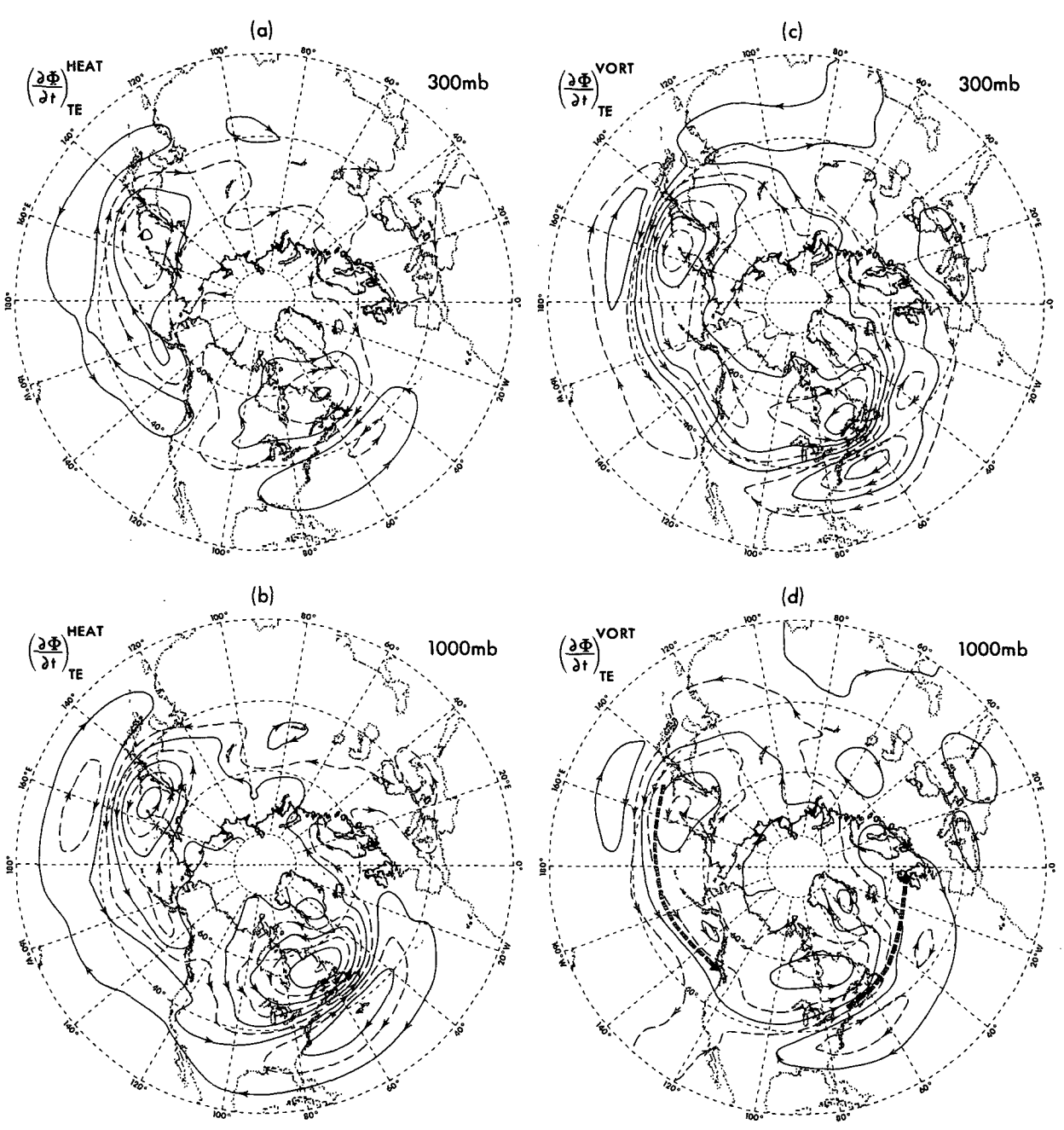


FIG. 3. Distributions of the geopotential tendencies associated with TE heat fluxes at (a) 300 mb and (b) 1000 mb, and with TE vorticity fluxes at (c) 300 mb and (d) 1000 mb. The eddy forcings are computed using band pass filtered data. Interval between solid contours is $5 \times 10^{-4}$ m$^2$ s$^{-3}$. Thin arrow heads indicate the direction of geostrophic wind tendencies. Thick arrows with dashed shafts in (d) indicate the axis of the principal wintertime storm tracks, as inferred from root-mean-square statistics of band pass filtered data (Blackmon *et al.*, 1977).

with TE fluxes of vorticity and heat tend to reinforce each other in the lower troposphere (Figs. 3b and 3d). The effects of eddy heat transports are relatively stronger at these levels. In the upper troposphere, the tendencies associated with eddy transports of vorticity and heat are seen to oppose each other, with the vorticity transports having a more dominating influence (Figs. 3a and 3c). The above results are more clearly illustrated by the longitude–pressure distributions of zonal wind tendencies along 40°N latitude, shown in

Fig. 4. It is seen from Fig. 4a that the strongest eastward and westward accelerations due to TE heat fluxes occur at 1000 and 200 mb, respectively. The forcing by vorticity transports tends to retain the same sign at all levels, with strongest magnitudes at 250 mb (Fig. 4b). Also evident in Fig. 4b is the transition from eastward acceleration at the beginning of the Atlantic storm track (90 to 50°W) to westward acceleration over the sector extending from 40 to 20°W. The total effect of the heat and vorticity fluxes is presented in Fig. 4c. The strongest eastward accelerations are seen to occur over the western portion of the Pacific and Atlantic storm tracks. The vertical variation at these locations is characterized by a primary maximum at 1000 mb and a secondary maximum near the tropopause, with typical magnitudes of 1–3 m $s^{-1}$ $day^{-1}$.

Hoskins *et al.* (1983) and A have also obtained the streamfunction tendency (denoted as $\psi^{VORT}$ in A and $S$ in Hoskins *et al.*) associated with TE vorticity fluxes by solving a two-dimensional Poisson's equation of the form

$$\nabla^2\psi^{VORT} = D^{VORT}$$

or

$$\nabla^2 S = D^{VORT}.$$

The results presented in these studies (see Fig. 6, lower right panel in A and Figs. 5a and 5b in Hoskins *et al.*) are similar to the patterns for $(\partial\Phi/\partial t)_{TE}^{VORT}$ shown in Figs. 3c and 3d here. The distributions of geopotential and wind tendencies along the storm tracks, as given in Figs. 3 and 4 here, are also in qualitative agreement with the results reported by Hoskins *et al.* (1983, Figs. 7a and 13).

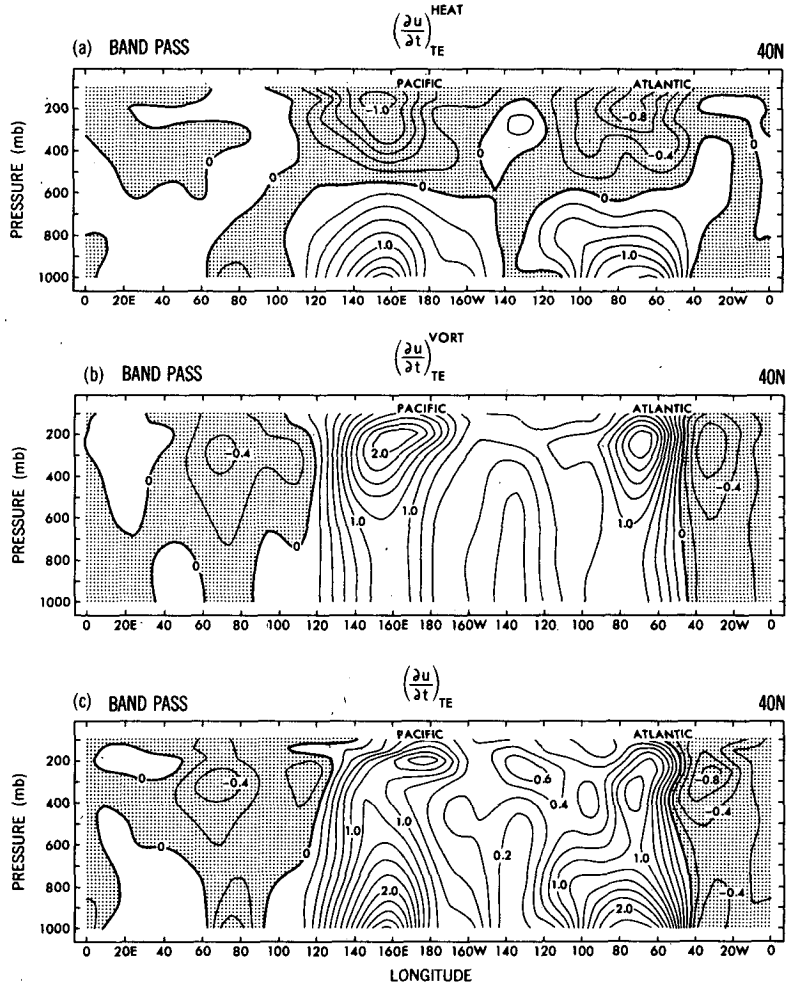


FIG. 4. Longitude-pressure distributions at 40°N of the zonal geostrophic wind tendencies associated with (a) TE heat fluxes, (b) TE vorticity fluxes and (c) sum of TE heat and vorticity fluxes. The eddy forcings are computed using band pass filtered data. Contour interval is 0.2 m $s^{-1}$ $day^{-1}$. Shading indicates negative values.

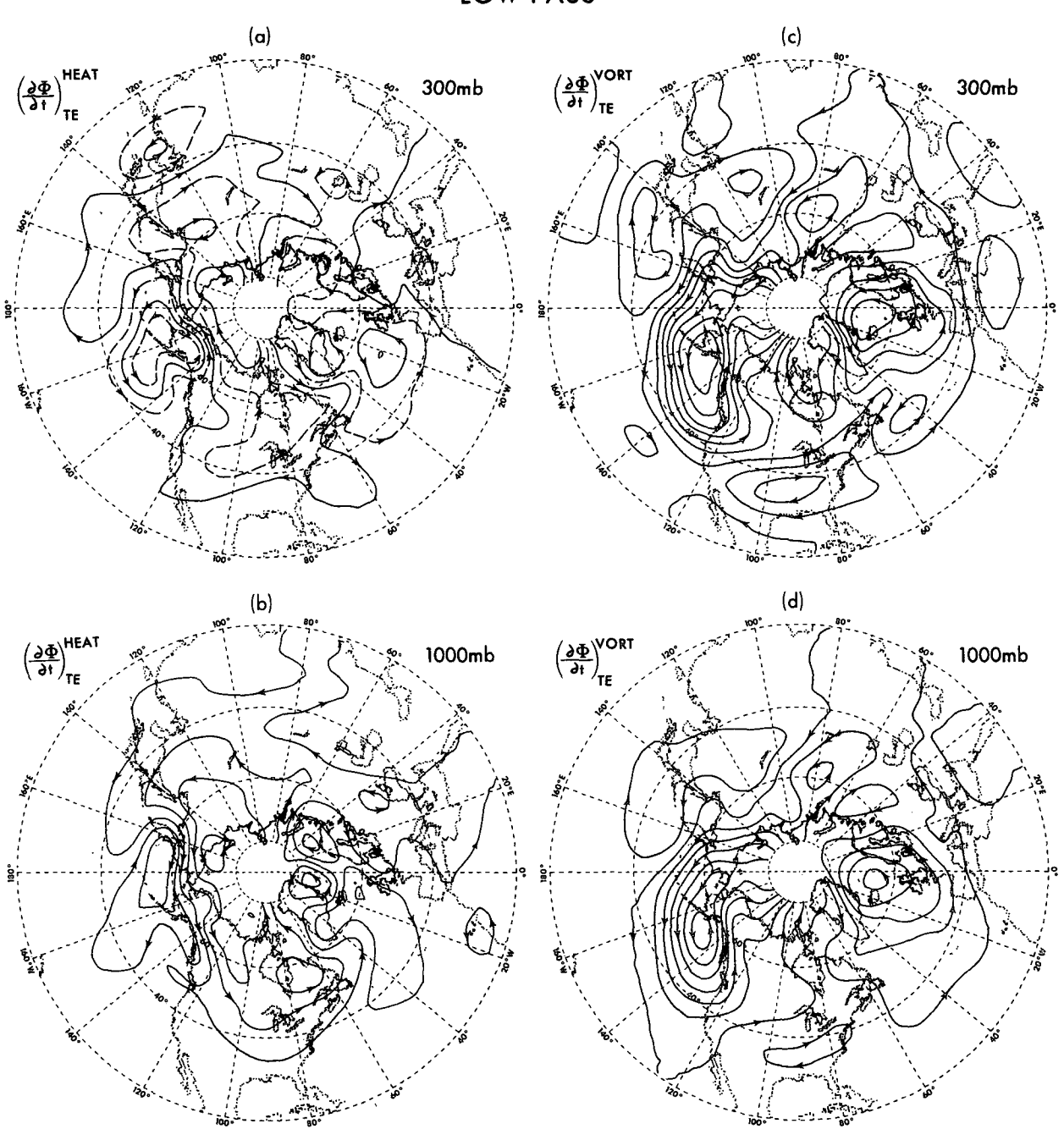


FIG. 5. As in Fig. 3, but for eddy forcings computed using low pass filtered data. Interval between solid contours is $5 \times 10^{-4}$ m$^2$ s$^{-3}$.

*b. Low-pass fluctuations*

The distributions of $(\partial\Phi/\partial t)^{HEAT}_{TE}$ and $(\partial\Phi/\partial t)^{VORT}_{TE}$ at 300 and 1000 mb, as computed using low-pass filtered eddy statistics, are displayed in Fig. 5. In the upper troposphere (Figs. 5a and 5c), the TE fluxes of heat and vorticity both act to force cyclonic circulations over the northeastern portion of the Atlantic and Pacific basins. Further west and southwest of the above features are regions mostly characterized by relatively weaker anticyclonic tendencies. The sites of these cyclonic and anticyclonic tendencies coincide, respectively, with the locations of the ridges and troughs in the time-averaged 300 mb height field (e.g., see Lau, 1979, Fig. 6b). The low-frequency fluctuations hence act to diminish the amplitude of the stationary waves in the upper tro-

# TOTAL

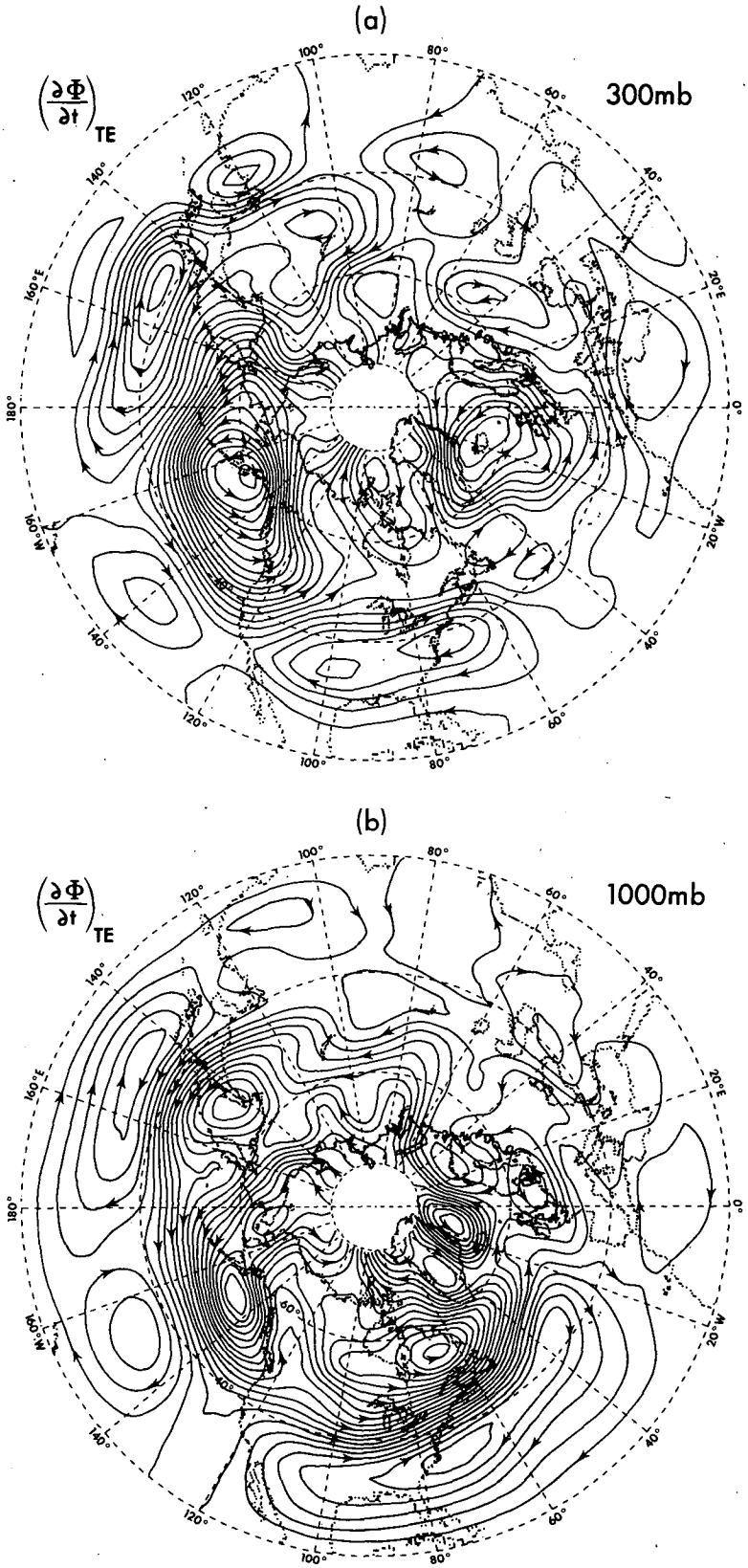
(a)
$\left(\frac{\partial \Phi}{\partial t}\right)_{TE}$
300mb
(b)
$\left(\frac{\partial \Phi}{\partial t}\right)_{TE}$
1000mb

posphere. The tendencies associated with vorticity fluxes at 300 mb are stronger than those associated with heat fluxes. In the lower troposphere (Figs. 5b and 5d), the polarity of the tendencies associated with heat fluxes is opposite to that at 300 mb, whereas the response to vorticity transports is very similar to that at the higher levels. The pattern in Fig. 5d suggests that TE vorticity fluxes tend to reinforce the eastern portion of quasi-permanent low pressure centers over Iceland and the Aleutians.

Contrary to the band pass patterns shown in Figs. 3c and 3d, the vorticity transports by the low-frequency eddies lead to strongest eastward accelerations near the eastern end of the oceanic storm tracks (Figs. 5c and 5d). Near the beginning of the storm tracks (at 45°N, 50°W and 35°N, 160°E), there are some indications that the vorticity transports act to decelerate the local westerly flow. The band pass and low pass patterns are also different in one other aspect: Fig. 3 indicates that $(\partial\Phi/\partial t)_{TE}^{HEAT}$ and $(\partial\Phi/\partial t)_{TE}^{VORT}$ for band pass eddies tend to oppose each other in the upper troposphere, and reinforce each other in the lower troposphere; whereas the reverse situation seems to hold for the low-pass eddies, with mostly cooperating tendencies at 300 mb and cancelling tendencies at the lower levels (Fig. 5).

The patterns for $(\partial\Phi/\partial t)_{TE}^{VORT}$ in Figs. 5c and 5d are similar to the corresponding results for streamfunction tendencies presented by A (Fig. 6, upper right panel) and Hoskins *et al.* (1983, Fig. 5c and 5d). The nature of the zonal flow forcing by the low pass eddies along the storm tracks is also in conformity with the pertinent discussion of Hoskins *et al.* (1983, Figs. 7b and 14).

### *c. Fluctuations of all time scales shorter than a season*

Comparison between the corresponding patterns in Figs. 3 and 5 reveals that tendencies associated with low-frequency eddies are generally stronger than those associated with synoptic scale disturbances. It is hence anticipated that the distributions of $(\partial\Phi/\partial t)_{TE}^{HEAT}$ and $(\partial\Phi/\partial t)_{TE}^{VORT}$ due to eddies of all time scales are dominated by contributions from the low-pass eddies. In Fig. 6 are shown the patterns of $(\partial\Phi/\partial t)_{TE}^{HEAT} + (\partial\Phi/\partial t)_{TE}^{VORT}$, as computed using unfiltered data, at 300 and 1000 mb. The features at 300 mb (Fig. 6a) are very similar to those appearing in $(\partial\Phi/\partial t)_{TE}^{VORT}$ for low pass eddies (Fig. 5c), thus indicating the importance of vorticity transports by slowly varying fluctuations in the upper troposphere. The net result of partial cancellations between $(\partial\Phi/\partial t)_{TE}^{HEAT}$ and $(\partial\Phi/\partial t)_{TE}^{VORT}$ for low pass eddies at 1000 mb (Figs. 5b and 5d) is a pattern characterized by eastward wind accelerations along a zonal belt extending eastward from Japan to the central Atlantic (Fig. 6b).

## 6. Regional characteristics of temperature tendencies

In Fig. 7 are shown the distributions of $(\partial T/\partial t)_{TE}^{HEAT}$ at 700 mb, for (a) band pass and (b) low pass disturbances. These patterns are obtained from $(\partial\Phi/\partial t)_{TE}^{HEAT}$ using the hydrostatic relationship. The temperature tendencies associated with vorticity fluxes $(\partial T/\partial t)_{TE}^{VORT}$ (not shown) are much weaker than the corresponding values for $(\partial T/\partial t)_{TE}^{HEAT}$. The patterns in Fig. 7 are qualitatively similar to those in the corresponding patterns for $(\partial\Phi/\partial t)_{TE}^{HEAT}$ (Figs. 3a, 3b, 5a and 5b). It is seen from Fig. 7a that the synoptic scale eddies exert the strongest influences on the thermal field in the vicinity of the storm tracks. By warming those regions located north of the axis of maximum cyclone activity and cooling the regions further south, the band pass fluctuations in effect act to reduce the meridional temperature gradient across the cyclone tracks. The corresponding pattern for low-pass eddies (Fig. 7b) exhibits a strong degree of zonal asymmetry, with positive temperature tendencies over the northeastern portion of Siberia and Canada, and negative tendencies over the Gulf of Alaska and northeastern Atlantic. A strong negative spatial correlation exists between the pattern in Fig. 7b and the zonally asymmetric component of the time averaged temperature field (e.g., see Lau, 1979, Fig. 1). The low-frequency eddies hence constitute an effective sink for the available potential energy of the stationary waves.

In Fig. 8a is shown the 700 mb distribution of $(\partial T/\partial t)_{TE}$ associated with both heat and vorticity transports by eddies of all time scales shorter than a season. This pattern bears a considerable resemblance to $(\partial T/\partial t)_{TE}^{HEAT}$ for low pass eddies (Fig. 7b). It is of interest to compare the features in $(\partial T/\partial t)_{TE}$ with those in the distribution for the convergence of TE heat fluxes $-\nabla\cdot\overline{\mathbf{V}'T'}$ at 700 mb. The latter pattern, shown in Fig. 8b, is obtained by Fourier analysis of values of $-\nabla\cdot\overline{\mathbf{V}'T'}$ along each latitude circle, and then retaining the zonal mean and the first ten zonal wavenumbers. An identical smoothing procedure has been performed in constructing the eddy forcing function for $(\partial\Phi/\partial t)_{TE}$ (see Section 4). Recalling that the effects of TE flux convergence and the associated secondary circulation have both been considered in computing $(\partial T/\partial t)_{TE}$, the differences between Figs. 8a and 8b may be attributed to the effects of the secondary circulation associated with the TE fluxes. It is seen that whereas the

FIG. 6. Distributions of the geopotential tendencies associated with the sum of TE heat and vorticity fluxes, at (a) 300 mb and (b) 1000 mb. The eddy forcings are computed using unfiltered data. Contour interval is $5 \times 10^{-4}$ m$^2$ s$^{-3}$. Arrow heads indicate the direction of geostrophic wind tendencies.

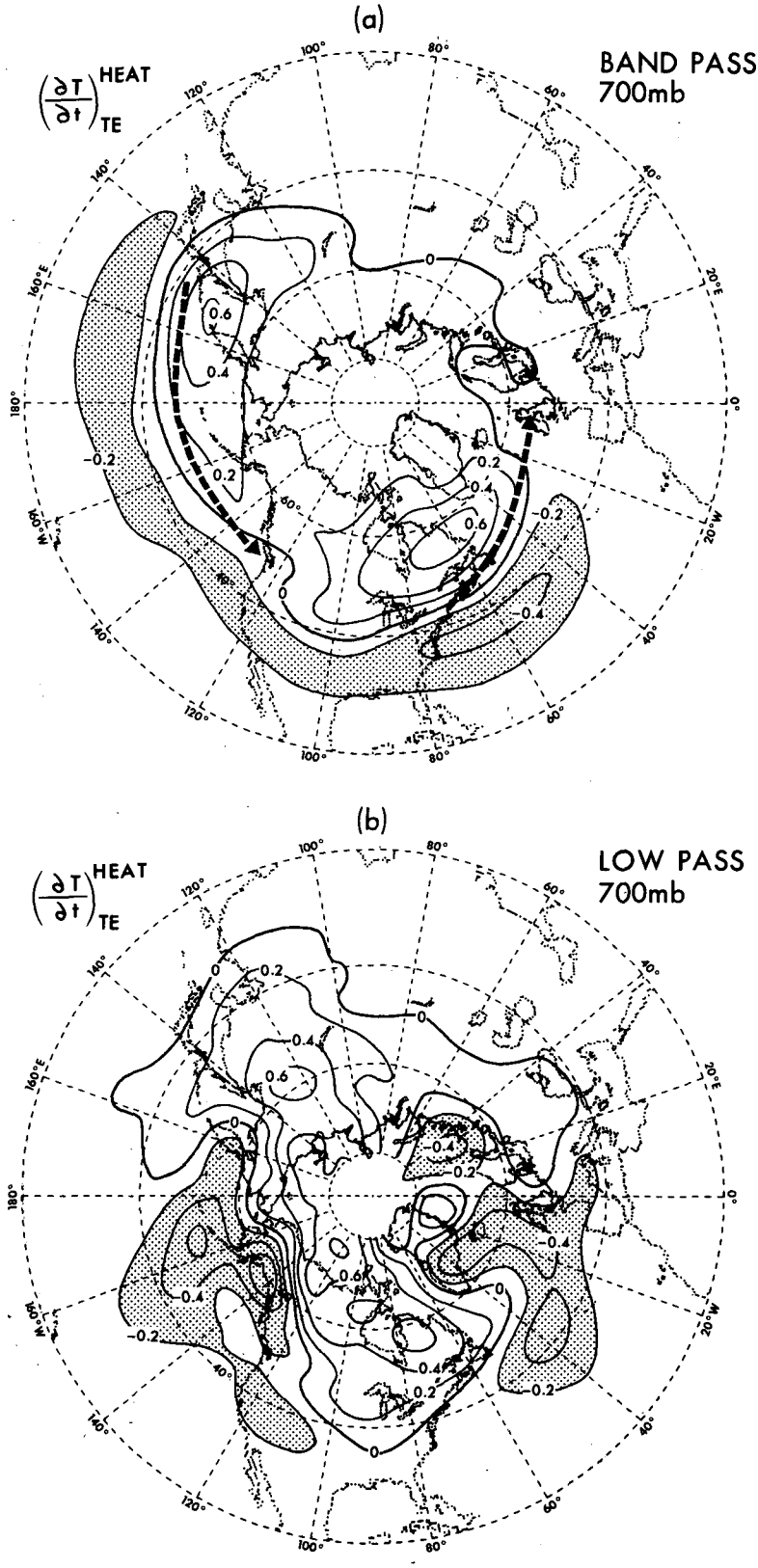


FIG. 7. Distributions of the temperature tendencies associated with TE heat fluxes at 700 mb, as computed using (a) band pass and (b) low-pass filtered data. Contour interval is 0.2°C day$^{-1}$. Thick arrows with dashed shafts in (a) indicate the axis of the principal wintertime storm tracks. Regions with cooling tendencies in excess of 0.2°C day$^{-1}$ are shaded.

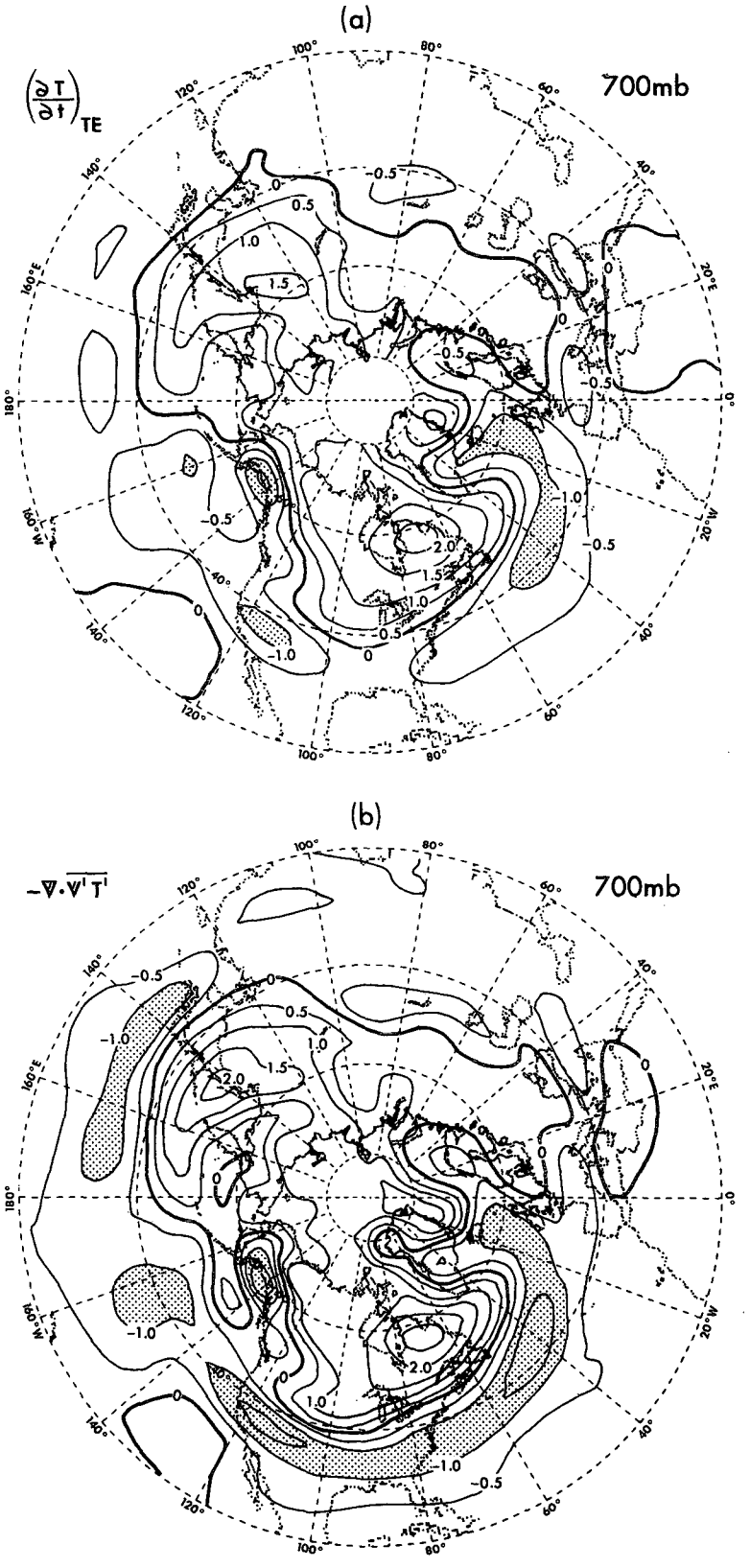


FIG. 8. Distributions of (a) temperature tendencies associated with TE heat and vorticity transports and (b) convergence of TE heat fluxes. Both patterns are obtained using unfiltered data at 700 mb. The pattern in (b) has been smoothed by a Fourier filter retaining the zonal mean and the first ten zonal wavenumbers. Contour interval is 0.5°C day$^{-1}$. Regions with cooling tendencies in excess of 1.0°C day$^{-1}$ are shaded.

two patterns in Fig. 8 are qualitatively similar to each other, the magnitudes of extrema in $(\partial T/\partial t)_{TE}$ are typically 60–70% of the corresponding values in $-\nabla \cdot \overline{\mathbf{V}'T'}$. The secondary circulations hence act to partially offset the effects due to convergences of TE eddy transports.

## 7. Zonally averaged distributions of zonal wind and temperature tendencies

The zonal mean patterns of the zonal wind accelerations due to transports of heat and vorticity by eddies of all time scales shorter than a season; $(\partial[u]/\partial t)_{TE}^{HEAT}$ and $(\partial[u]/\partial t)_{TE}^{VORT}$, are displayed in Fig. 9. Results for band pass and low pass statistics (not shown) are qualitatively similar to those presented here. Within the zone between 35 and 55°N, the TE heat fluxes are associated with eastward acceleration in the lower troposphere, and westward acceleration in the upper troposphere (Fig. 9a). The vorticity transports tend to strengthen the westerlies at all levels in the middle latitudes, whereas the zonal mean flow in the subtropics and polar latitudes experiences westward acceleration (Fig. 9b). The sum of $(\partial[u]/\partial t)_{TE}^{HEAT}$ and $(\partial[u]/\partial t)_{TE}^{VORT}$, shown in Fig. 9c, is characterized by maximum westerly tendencies near 45°N, and at the 1000 and 200 mb levels. The strongest accelerations hence occur poleward of the climatological position (at 200 mb and 32.5°N) of the zonal mean jet.

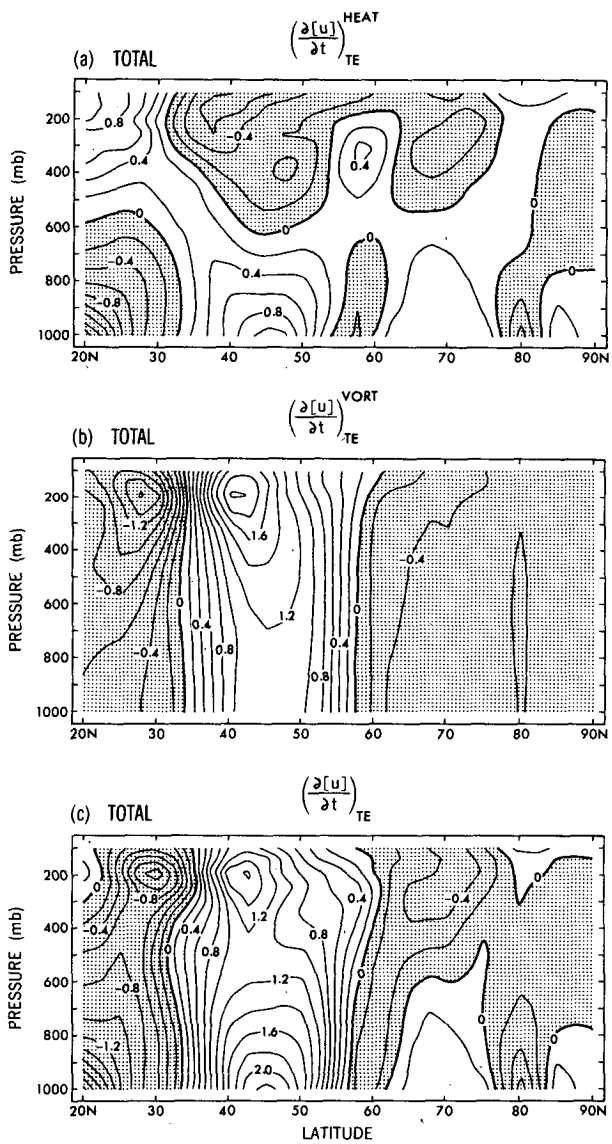


FIG. 9. Latitude-pressure distributions of the tendencies of zonally averaged zonal geostrophic wind associated with (a) TE heat fluxes, (b) TE vorticity fluxes and (c) sum of TE heat and vorticity fluxes. The eddy forcings are computed using unfiltered data. Contour interval is 0.2 m $s^{-1}$ $day^{-1}$. Shading indicates negative values.

By averaging the time mean zonal momentum equation over longitude and pressure, it can be shown that

$$\left(\frac{\partial\widehat{[u]}}{\partial t}\right)_{TE}^{HEAT} = 0, \quad \left(\frac{\partial\widehat{[u]}}{\partial t}\right)_{TE}^{VORT} = -\frac{\partial}{\partial y}\widehat{[u'v']},$$

where the caret represents average over the entire atmospheric column, and the parentheses denote zonal average. It has been verified by direct computations (not shown) that the results presented in this section satisfy the above relationships to a high degree of accuracy. These constraints also imply that the TE heat fluxes can only alter the baroclinic component of the zonal mean flow, as is evident from inspection of Fig. 9a.

A pattern similar to that shown in Fig. 9c has been presented by Pfeffer (1981, Fig. 8, third panel). In the latter study, the net eddy forcing of the zonal mean flow was computed by summing the convergence of eddy momentum flux and the Coriolis force accompanying the eddy-induced meridional circulation. The results thus obtained are in qualitative agreement with those exhibited in Fig. 9c here. The dissimilarities between the results in this and Pfeffer's studies are probably attributable to inclusion of stationary eddy effects in Pfeffer's study, as well as to differences in the data base and numerical procedures used.

In Fig. 10 are shown the zonally averaged distributions of temperature tendencies associated with TE fluxes of heat and vorticity, as computed using unfiltered statistics. The pattern for $(\partial[T]/\partial t)_{TE}^{HEAT}$ (Fig. 10a) is characterized by negative tendencies equatorward of 45°N, and positive tendencies further north. The strongest warming and cooling occur in the lower troposphere, with maximum amplitudes of 0.5–1 °C $day^{-1}$. The temperature tendencies associated with vorticity fluxes are relatively much weaker. The pattern in Fig. 10b suggests that the TE vorticity fluxes are accompanied by a thermally indirect circulation in the middle latitudes, with ascending motion (cooling) near 60°N and descending motion (warming) near 35°N. The tendencies associated with both heat and vorticity fluxes (Fig. 10c) are dominated by the contribution of

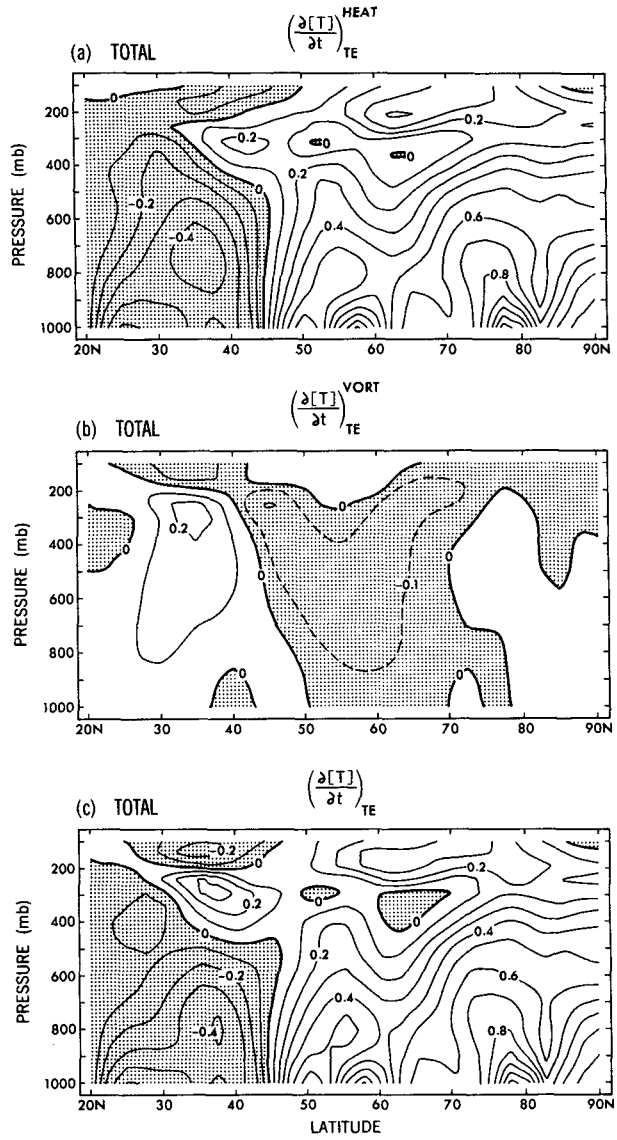


FIG. 10. As in Fig. 9, but for tendencies of zonally averaged temperature. Contour interval is 0.1°C day$^{-1}$.

the heat fluxes. The essential features in Fig. 10c are qualitatively similar to those presented by Pfeffer (1981, Fig. 11, third panel).

## 8. Distinguishing two representations of TE effects—tendencies associated with eddy transports versus potential vorticity fluxes

In our previous study A, the TE effects were depicted using a streamfunction $\psi$ satisfying the relationship $\nabla^2\psi = D$. A nondivergent vector field $\mathbf{F}_\psi$ may then be defined such that $\mathbf{F}_\psi = \mathbf{k} \times \nabla\psi$. To a good approximation, $D$ may be expressed as $D = -\nabla \cdot \overline{\mathbf{V}'q'}$, where $q$ is one form of quasi-geostrophic potential vorticity [see A, Eq. (6b)]. Hence $\psi$ may be viewed as the potential function for the irrotational component of $\overline{\mathbf{V}'q'}$, so that $(\overline{\mathbf{V}'q'})_\chi = -\nabla\psi$. Here the subscript $\chi$ denotes the irrotational component. $\mathbf{F}_\psi$ is therefore related to $(\overline{\mathbf{V}'q'})_\chi$ by

$$\mathbf{F}_\psi = (\overline{\mathbf{V}'q'})_\chi \times \mathbf{k}. \tag{9}$$

The vector field $\mathbf{F}_\psi$ as described in A and the geostrophic wind tendency $(\partial\mathbf{V}/\partial t)_{TE}$ computed in the present paper both purport to represent TE forcing of the time mean flow. Yet these two quantities are characterized by quite dissimilar spatial patterns. That this is so can be appreciated by contrasting the hemispheric distributions of $\psi$ (Fig. 4c in A) and $(\partial\Phi/\partial t)_{TE}$ (Fig. 6, this paper), as well as the zonally averaged sections of $\mathbf{F}_\psi$ (Fig. 2 in A) and $(\partial[u]/\partial t)_{TE}$ (Fig. 9, this paper). Hence $\mathbf{F}_\psi$ and $(\partial\mathbf{V}/\partial t)_{TE}$ apparently illustrate different aspects of the TE forcing. In this section, the distinctions between these two methodologies are highlighted by discerning the individual roles of potential vorticity fluxes and $(\partial\mathbf{V}/\partial t)_{TE}$ in atmospheric energetics.

### a. *TE potential vorticity fluxes*

By manipulations analogous to those outlined in Pfeffer (1981, Appendix), it can be shown that, for quasi-nondivergent motions satisfying the thermal wind relationship, we have

$$\langle -\bar{u}\overline{v'q'} + \bar{v}\overline{u'q'}\rangle = \langle \mathbf{k} \cdot \overline{\mathbf{V}'q'} \times \bar{\mathbf{V}}\rangle = C(K_M, K_{TE}) + C(P_M, P_{TE}) + R_3. \tag{10}$$

Here the angle braces denote a volume integral over the entire atmosphere, the first and second term on the right hand side of Eq. (10) represent conversion of kinetic energy and available potential energy, respectively, from the time mean flow to the transient eddies, and $R_3$ represent terms involving heat fluxes at the upper and lower boundaries. Simple order-of-magnitude estimates based on representative observed values indicate that the contribution of $R_3$ is generally small compared with the conversion terms. Furthermore, using the relationship expressed in Eq. (9), the left-hand side of Eq. (10) may be rewritten as

$$\langle \mathbf{k} \cdot \overline{\mathbf{V}'q'} \times \bar{\mathbf{V}}\rangle = \langle \mathbf{k} \cdot (\overline{\mathbf{V}'q'})_\chi \times \bar{\mathbf{V}}\rangle = -\langle \bar{\mathbf{V}} \cdot \mathbf{F}_\psi\rangle. \tag{11}$$

It is obvious from Eqs. (10) and (11) that the dot product of the vector field $\mathbf{F}_\psi$ with the local time-mean flow is a measure of the TE effects in generating or destroying the total energy $P_M + K_M$ in the time mean flow. As has been demonstrated in A (Figs. 4c and 4d), $\mathbf{F}_\psi$ is directed against $\mathbf{V}$ almost everywhere in the Northern Hemisphere, i.e., $\langle \mathbf{V} \cdot \mathbf{F}_\psi\rangle < 0$, the transient eddies hence constitute an effective sink for the total energy of the stationary flow. Noting that the magnitude of $C(P_M, P_{TE})$ is much greater than that of $C(K_M, K_{TE})$ [e.g., see Lau and Oort (1982, Fig. 13 and Table 1)], we would expect the essential features of $\mathbf{F}_\psi$ to be largely dictated by the action of the eddies to deplete $P_M$. Since such dissipative effects are to be accomplished by the eddy transports of heat down the

local temperature gradient, we would also expect $\mathbf{F}_\psi$ to be dominated by that component which portrays the effects of eddy heat fluxes, i.e., $\mathbf{F}_\psi^{HEAT}$ [see definition in Eq. (9) of A]. The results displayed in A (Figs. 4 and 6) demonstrate that this is indeed the case.

*b. Geostrophic wind and temperature tendencies associated with eddy transports*

The interpretation for $(\partial\Phi/\partial t)_{TE}$ and $(\partial T/\partial t)_{TE}$ as described in this paper is relatively straightforward. The wind tendencies at a given level (Figs. 3, 5 and 6) depict the effects of eddy fluxes on the local velocity field alone, and provide no information on the eddy forcing of the thermal field. The nature of the latter effects is revealed by the patterns of $(\partial T/\partial t)_{TE}$ (Figs. 7 and 8a). As has been pointed out in the preceding sections, $(\partial \mathbf{V}/\partial t)_{TE}$ tends to oppose the velocity field of the stationary waves in the upper troposphere (Fig. 6a); and $(\partial T/\partial t)_{TE}$ acts to destroy the meridional temperature gradient of the zonally averaged flow (Fig. 10c), as well as the departure from zonal symmetry of the time averaged temperature field (Fig. 8a). Hence, despite the apparent difference in the patterns of $\mathbf{F}_\psi$ and $(\partial \mathbf{V}/\partial t)_{TE}$, the two approaches adopted in A and in this paper lead to essentially the same conclusion, *i.e.*, that TE serve as an effective damping mechanism for the time mean flow.

In summary, we have offered two diagnostic tools for identifying TE effects on the time mean flow. The first method was introduced in A, and involves the mapping of the field $\psi$ (or the associated vector field $\mathbf{F}_\psi$) at a given pressure level. This single quantity depicts the influences of the eddies on both the velocity and temperature structures of the stationary flow. The second method, as outlined in this paper, entails the mapping of two different fields $(\partial \mathbf{V}/\partial t)_{TE}$ and $(\partial T/\partial t)_{TE}$ for each pressure level, which portray the eddy forcing of the velocity and temperature structures, respectively.

## 9. Concluding remarks

In this paper, an attempt has been made to describe the initial tendencies experienced by an atmosphere in response to empirically determined sources and sinks of heat and vorticity associated with systematic TE transports. As one interprets the results presented here, it is necessary to bear in mind that such tendencies would eventually lead to responses of sufficient amplitude to be of importance in ageostrophic and nonconservative processes not yet considered here, such as advection, friction and diabatic heating. Further insight into this problem might be gained by examining the stationary, finite-amplitude response to the eddy forcing. It is, however, noteworthy that both the tendencies described here and the steady-state solutions reported by Youngblut and Sasamori (1980) and Opsteegh and Vernekar (1982) indicate that TE act to dissipate the stationary waves. The initial tendencies discussed here may hence be used as a tool for diagnosing and verifying the results of various numerical and theoretical studies on eddy-mean flow interactions.

*Acknowledgments.* We wish to thank Drs. Y. Hayashi, I. M. Held, J. D. Mahlman, A. H. Oort and G. H. White for examining the manuscript and for offering helpful comments. We are also indebted to Ms. J. Callan for typing the manuscript, and to Messrs. J. Connor, W. Ellis and P. Tunison of the Geophysical Fluid Dynamics Laboratory for preparing the figures. NCL is supported at the Geophysical Fluid Dynamics Program by NOAA Grant 04-7-022-44017.

## REFERENCES

Blackmon, M. L., 1976: A climatological spectral study of the 500 mb geopotential height of the Northern Hemisphere. *J. Atmos. Sci.*, **33**, 1607–1623.

——, J. M. Wallace, N-C. Lau and S. L. Mullen, 1977: An observational study of the Northern Hemisphere wintertime circulation. *J. Atmos. Sci.*, **34**, 1040–1053.

Bretherton, F. B., 1966: Critical layer instability in baroclinic flows. *Quart. J. Roy. Meteor. Soc.*, **92**, 325–334.

Edmon, H. J., B. J. Hoskins and M. E. McIntyre, 1980: Eliassen-Palm cross-sections for the troposphere. *J. Atmos. Sci.*, **37**, 2600–2616.

Holopainen, E. O., L. Rontu and N-C. Lau, 1982: The effect of large-scale transient eddies on the time-mean flow in the atmosphere. *J. Atmos. Sci.*, **39**, 1972–1984.

Holton, J. R., 1979: *An Introduction to Dynamic Meteorology*, 2nd ed. Academic Press, 391 pp.

Hoskins, B. J., I. N. James and G. H. White, 1983: The shape, propagation and mean-flow interaction of large-scale weather systems. *J. Atmos. Sci.*, **40**, 1595–1612.

Lau, N-C., 1979: The observed structure of tropospheric stationary waves and the local balances of vorticity and heat. *J. Atmos. Sci.*, **36**, 996–1016.

——, and J. M. Wallace, 1979: On the distribution of horizontal transports by transient eddies in the Northern Hemisphere wintertime circulation. *J. Atmos. Sci.*, **36**, 1844–1861.

——, and A. H. Oort, 1982: A comparative study of observed Northern Hemisphere circulation statistics based on GFDL and NMC analyses. Part II: Transient eddy statistics and the energy cycle. *Mon. Wea. Rev.*, **110**, 889–906.

——, G. H. White and R. L. Jenne, 1981: Circulation statistics for the extratropical Northern Hemisphere based on NMC analyses. NCAR Tech. Note 171 + STR, 183 pp.

NCAR Software Support Library, 1976: Vol. II. NCAR Tech. Note TN/IA-105.

Opsteegh, J. D., and A. D. Vernekar, 1982: A simulation of the January standing wave pattern including the effects of transient eddies. *J. Atmos. Sci.*, **39**, 734–744.

Pfeffer, R. L., 1981: Wave-mean flow interactions in the atmosphere. *J. Atmos. Sci.*, **38**, 1340–1359.

Wiin-Nielsen, A., and A. D. Vernekar, 1967: On the influence of the mean meridional circulation on the zonal flow. *Mon. Wea. Rev.*, **95**, 723–732.

Youngblut, C., and T. Sasamori, 1980: The nonlinear effects of transient and stationary eddies on the winter mean circulation. Part I: Diagnostic analysis. *J. Atmos. Sci.*, **37**, 1944–1957.